Large-Scale Molecular Dynamics Simulations of Early- and Intermediate-Stage Sintering of Nanocrystalline SiC

Bryce D. Devine, Jeffrey B. Allen, Charles F. Cornwell, and Charles R. Welch

Engineer Research and Development Center, US Army Corp of Engineers, Vicksburg, MS

{Bryce.D.Devine, Jeffrey.B.Allen, Charles.F.Cornwell, Charles.R.Welch}@usace.army.mil

Abstract

Polycrystalline silicon carbide (SiC) has tremendous potential as a lightweight structural material if its fracture toughness and tensile strength could be significantly (factor of 4) improved, which is the long-term goal of this and related research. Such a "super" ceramic would allow for two-thirds weight reduction, or more, over that of steel and aluminum for most structural applications. The potential impact on military logistics is enormous. Key to the realization of such a super ceramic is the development of appropriate SiC composite designs and the development of methods to fabricate SiC composites to meet these designs through sintering. Technologies to support SiC composite design development are addressed in a companion paperThis paper discusses research to develop sintering fabrication methods. Recently developed sintering techniques allow for the production of ceramic materials with nanocrystalline grain structures and for the incorporation of organic reinforcements in ceramic composites. Both reduction in grain size and the incorporation of tensile members have been shown to improve the fracture toughness of SiC. We are performing multi-million-atom classical molecular dynamics (MD) simulations of early- and intermediate-stage Spark Plasma Sintering (SPS) of nanocrystalline SiC to better understand, and then engineer, the sintering process. We have developed continuum models to predict the thermal, electric, and displacement fields inside the sintering chamber. These provide boundary and initial conditions for the MD simulations of sintering. Several mechanisms were observed during each stage of sintering consolidation, with the rate limiting mechanism dependent upon temperature, pressure and grain size. This research helps lay the technical foundation for development of a lightweight structural "super" ceramic matrix composite.

1. Introduction

High-performance silicon carbide (SiC) ceramics are remarkably strong and lightweight materials, and potentially offer dramatic performance gains over current materials in structural applications. A few properties of current SiC-based materials are compared with other structural materials in Table 1. SiC ceramics are twice as stiff as steels, have three times the compressive strength of very high-strength steel yet are comparable in density to aluminum alloys (Howatson, Lund, and Todd 1991). The main limitation with ceramics materials in general is their relatively low fracture toughness and weak bending strength, which is related to the tensile strength. If the fracture toughness and tensile strength can be improved, SiC could replace steels and aluminum alloys many applications, at a fraction of the weight and possibly, at a fraction of the cost over the lifetime of the part.

Single-crystal SiC is very strong, with an ultimate tensile strength of 8.4 GPa (Petrovic, et al. 1985), more than 10 times that of high-strength steels. However, ceramic materials in application are polycrystalline, which exhibit considerably lower tensile strengths because of pores and micro-cracks that form within the matrix during synthesis. When overloaded, these defects in the microstructure act as stress risers leading to fracture and brittle failure at lower applied loads.

High-strength ceramic materials are produced by a sintering process, in which a green form consisting of a compacted powder is heated to and held at a temperature near the melting point. The individual particles in the green form fuse together to form a continuous solid network. Without modification, the process typically results in a porous microstructure

that is weak and brittle in tension. Application of pressure, called hot pressing, and the addition of sintering aids, such as lower melting point materials that form secondary liquid phases between grains, have greatly improved the density and consequently the performance of the sintered materials (Rahaman 2008).

Traditional liquid phase sintering methods have been optimized for SiC to the point at which the strength of the final materials is approaching the theoretical maximum of the single crystals. In these high-performance materials, fracture occurs along the shear planes within the individual SiC crystals rather than through the grain boundaries between crystals. Routes to further improvement are focused on optimizing the sintering process to produce strong defect-free crystals and inclusion of tougher materials as tensile reinforcements.

Table 1. Material properties of SiC compared with common structural materials.

Material	Young's Modulus (million psi)	Compressive Strength (ksi)	Density (lb/ft^3)	Fracture Toughness ($MPa\ m^{0.5}$)	Bending Strength (ksi)	Max Service Temp (F)
Silicon Carbide (SiC)	59.5	566	194	4.6	80	3000
Boron Carbide (B_4C)	63.8	560	157	3.1	62	1112
Aluminum Oxide (Al_2O_3)	43.5	305	230	3.5	47	3092
High Strength Steel (4340)	29.7	160 - 200	490	50	160 to 200	2600
Aluminum 7075-T6	10.4	74 - 78	170	24	74-78	900

One possible means to improve the strength of SiC is to maintain a nanocrystalline grain size during sintering. Hardness and strength have been shown to increase with decreasing grain size in SiC (Szlufarska, Nakano, and Vashishta 2005; Mo and Szlufarska 2007). During sintering, grain growth occurs concurrently with consolidation. Under conventional conditions, a nanocrystalline grain structure cannot be produced in the final product because of grain growth even when a finally graded, nanocrystalline powder is used as a starting material. Recently the development of field-assisted sintering techniques (FAST), also known as spark plasma sintering (SPS), allows for the production of nanocrystalline ceramics (Orru et al. 2009). During FAST processing, an external electric field is applied across the compacted powder while the powder is heated and pressed, which increases the densification rate and allows for sintering at lower temperatures, resulting in reduced grain growth. The lower processing temperature also allows for the inclusion of temperature-sensitive tensile phases such as carbon nanotubes.

As a fairly new technique, FAST sintering is not well understood from a mechanistic point. Some fundamental aspects of the process such as what effect the field provides and the atomic mechanism that leds to densification at lower temperature are yet to be confirmed (Langer, Hoffmann, and Guillon 2009). Multiscale modeling is being used to address theses basic questions about the process. Modeling efforts range from the atomistic to the continuum level. At the continuum scale, finite element modeling of the sintering chamber is being used to explore the temperature, electrical current, and stress distribution within the sample over time. The temperature and stress distributions set the boundary and initial conditions for the concurrent molecular dynamics simulations that identify the densification mechanisms that are rate limiting at various temperatures and grain sizes. Aspects of both these efforts are presented in this article.

2. Methods

2.1. Finite Element Modeling

Recently we developed a fully-integrated thermal/electrical/mechanical multi-physics model to explore the evolution of the temperature and stress fields within the sample during the consolidation process (Allen et al., forthcoming). The

model incorporates a Proportional Integral Derivative (PID) thermal controller (Munoz, et al. 2010) that allows for control over the heating rates and includes effects caused by contact forces, radiation, and Joule heating. Thermal control of the system requires a description of material properties that vary with temperature and density.

A schematic of the FAST apparatus modeled in this study is presented in Figure 1. The powder sample is held within a graphite die between two graphite punches. During sintering an electrical current is applied at high amperage and low voltage through the conductive punches and the sample being sintered. Pressure is concurrently applied to the sample to assist the consolidation process.

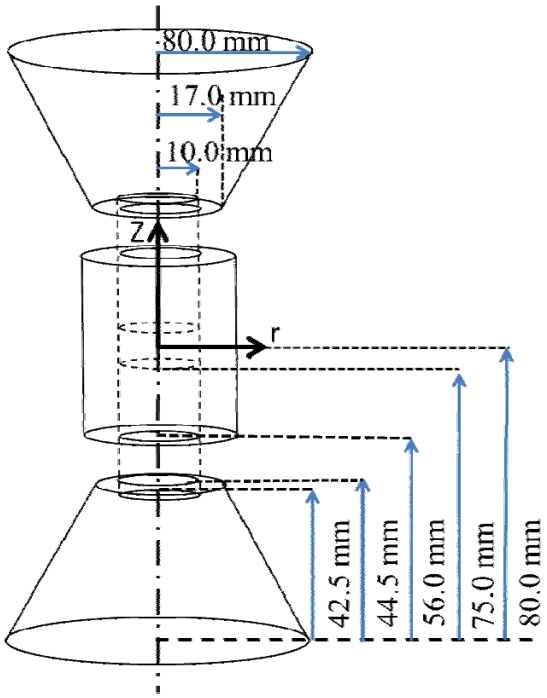

Figure 1. A wireframe schematic of the FAST apparatus (FCT HP 25/1, FCT, Germany) used in this study showing nominal dimensions and placement of the origin in cylindrical coordinates.

Comparisons of the model with experiments revealed excellent agreement in terms of quantifying the temperature evolution at a fixed point outside the sample. Within the sample, the numerical results show significant, non-homogeneous temperature and hydrostatic stress distributions, both decreasing with radial distance from the centerline of the sample toward the die interface. The significant thermal gradients that arise during the process are illustrated in the contour plots in Figure 2. Previous studies have indicated that these temperature and stress gradients could compromise the integrity of the material.

Current simulations are exploring the effect of densification kinetics within the model and reveal the importance of including such effects particularly during the early stages of sintering. The kinetic properties of the consolidation reactions within nanocrystalline SiC are unknown and are being explored through atomistic modeling.

2.2. Molecular Dynamics Simulations

The most computationally expensive portion of this work consists of molecular dynamics (MD) simulations of the sintering process. This process determines the atomic scale mechanisms that govern the consolidation reactions as a function of grain size and temperature. The complete sintering process occurs on the time scale of minutes, which is beyond the scope of atomic-scale simulations.

The sintering process is typically described in terms of three stages (Rahaman 2008). In the early or initial stage, necks form between separate particles and densification is governed by neck growth. Particles can slide and rotate to form lower energy interfaces that promote intergranular growth. As necks grow, the pore sizes are reduced. Migration of material to and from free surfaces is restricted. Densification becomes limited more by grain boundary and lattice diffusion. This diffusion-limited phase is characteristic of the intermediate stage of sintering. Pores remain interconnected

during the intermediate stage. Eventually, in the final stage of sintering the intergranular channels close off and form isolated pores. The kinetic phenomena in the final stage are typically modeled as those of the bulk material. Until the availability of current high-performance computing (HPC) systems, atomistic modeling of sintering was limited to the early-stage phenomena. However, intermediate-stage sintering processes can be observed on a time scale of a few nanoseconds, which is now quite tractable.

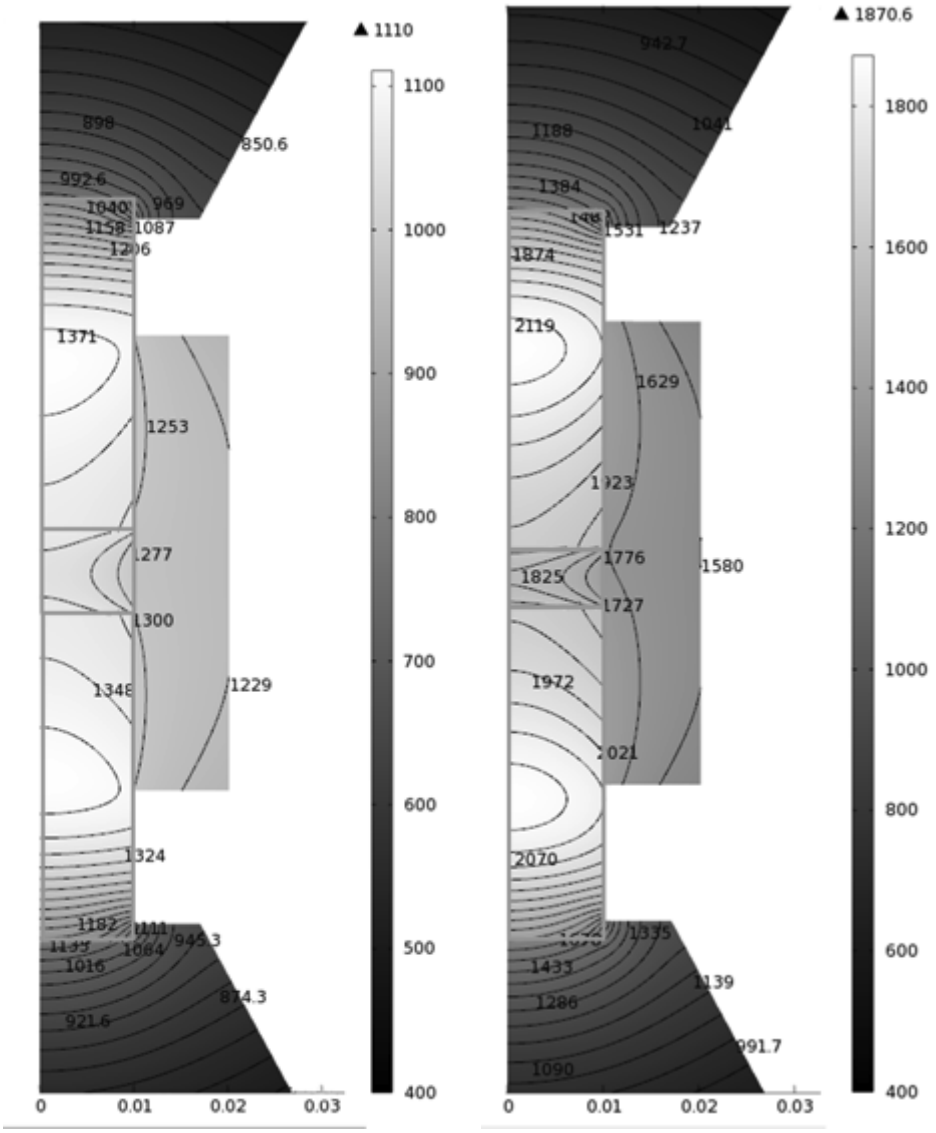

t=523 sec. t=838 sec.

Figure 2. Temperature contour plots corresponding to two time intervals: t=523 sec. and t=838 sec.

2.3. Molecular Dynamics Simulations Computational Details

All MD simulations were performed using the parallel COMB suites of codes developed at the University of Florida (Devine et al. 2011). A three-body Tersoff potential parameterized by Albe and Erhart for Si, C, and SiC was used to describe bonded interactions (Tersoff 1988; Erhart and Albe 2005). Simulations were performed in the constant temperature and pressure (NPT) ensemble. Temperature during sampling was controlled with a Nose-Hoover chain

thermostat, which has been shown to properly sample the statistical ensemble (Martyna, Klein, and Tuckerman 1992). Pressure was maintained through a Parrinello-Rahman dynamical bariostat with periodic boundary conditions applied in three dimensions (Parrinello and Rahman 1981).

The model system consisted of 32 spherical nano-crystals of 3C-SiC stacked in a cubic close-packed arrangement. Crystals are of equal size to minimize effects due to grain growth with sizes ranging from 3 nm to 20 nm in diameter. Crystals are randomly oriented relative to one another. Each crystal has 12 neighbors yielding 384 different interfaces. The largest systems in this study contain 16 million atoms.

During simulations, the systems are initially optimized via steepest descent algorithm and annealed at low temperature to eliminate erroneous high-energy configurations. The system is then heated to 300 K and compressed at 100 MPa to form a compacted green body. The compacted system wass heated to the sampling temperature and pressure at a rate of 1 K/ps and held for 5 ns.

3. Results and Discussion

Throughout the simulations, temperatures were reported as a fraction of melting point (T_m). Sintering data was collected at temperatures ranging from 0.5 to 0.8 T_m. A comparison of density over time at each temperature, which is plotted in Figure 3 for a system of 5 nm crystals, demonstrates that early and intermediate stage phenomena are exhibited on the time scale of MD. At lower temperatures, consolidation proceeds via neck growth. Initially, particles rotate to form lower energy interfaces. The combination of grain rotations and neck formation leads to an increased rate of densification in the first few hundred ps of the simulation. Once necks form, densification proceeds at comparable rates at temperature below 0.8 T_m.

The increased rate seen at 0.8 T_m in Figure 3 is attributed to melting at the particle surfaces, indicating 5-nm-diameter crystals are below the critical size at that temperature. A plot of density versus time at 0.8 T_m for larger crystals, shown in Figure 4, indicates that larger crystals are more stable at this temperature. Likewise, the surfaces of 3-nm crystals begin melting at temperatures below 0.6 T_m.

3.1. Early Stage Sintering Mechanisms

Early-stage neck formation was observed during the simulations. Figure 5 shows an image of a 10-nm system early in the simulation at 0.5 T_m. Color in the image indicates defects; orange atoms occupy sites of point defects or dislocations, grey atoms occupy normal lattice sites, and black atoms are undercoordinated. Neck formation occurs preferentially between favorably aligned interfaces and does not occur between misaligned interfaces. This is consequential since most early-stage models and current meso-scale models assume neck formation across all interfaces (Rahaman 2008). The material in the neck regions is perfectly crystalline, suggesting that material is moving into the neck region as vacancies move out, which is consistent with traditional models (Coble 1970). No defects are observed within the crystals, suggesting that densification at this temperature and stage occurs predominately via surface diffusion.

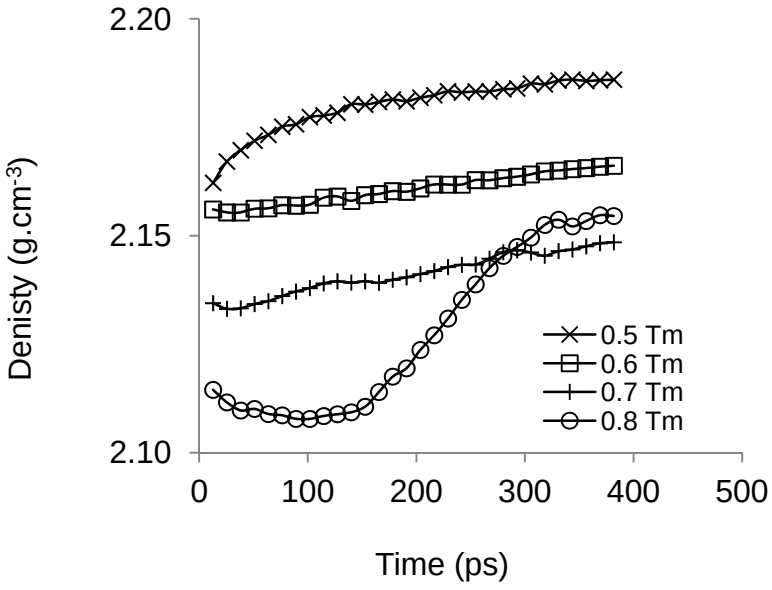

Figure 3. Density as a function of time for 5-nm sized crystals of 3C-SiC. The drop in density between temperatures is due to thermal expansion.

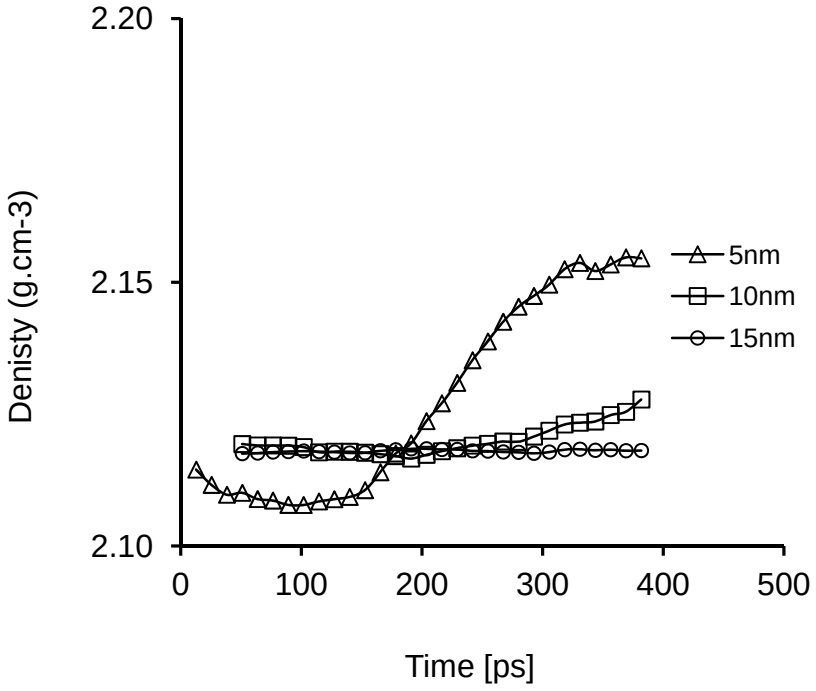

Figure 4. Density as a function of time at 0.8 T_m for various sized crystals.

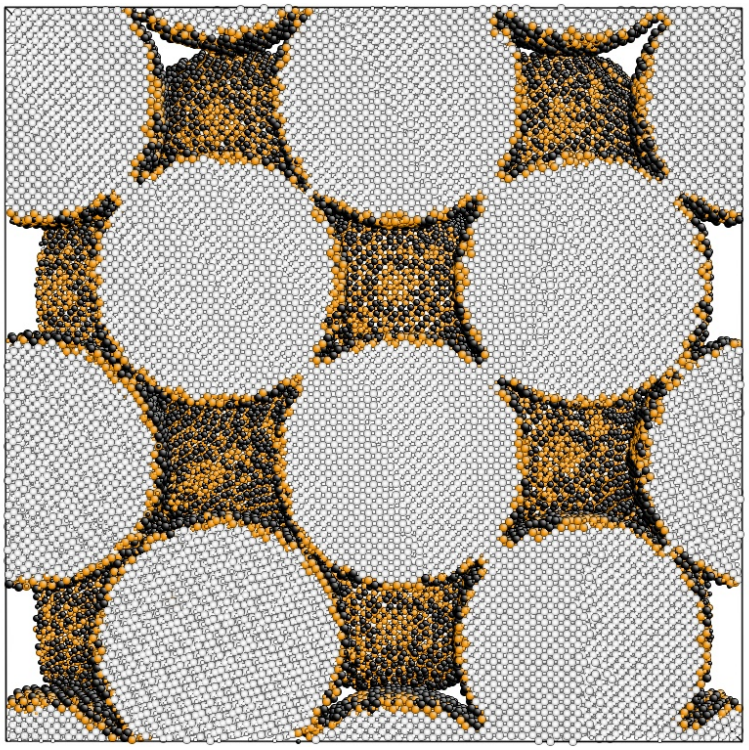

Figure 5. Neck formation and growth in 10-nm crystals of 3C-SiC at 0.5 T_m. Color indicates defects; black atoms are undercoordinated, orange atoms are dislocations or point defects, and grey atoms occupy normal lattice sites.

3.2. Intermediate Stage Sintering Mechanisms

Sintering is limited by diffusion with a rate equation that depends on the rate limiting diffusion mechanism. FAST sintering has been shown to follow similar rate behavior as hot pressing high pressure. In which case, the rate of densification is given by (Rahaman 2008; Coble 1970):

$$\frac{1}{\rho}\frac{d\rho}{dt} = \frac{HD\phi^n}{G^m kT} P_a^n \tag{1}$$

where ρ is the relative density, H is a constant, D is the diffusion coefficient, k is Boltzmann's constant, T is temperature, P_a is the applied pressure, G is the grain size, and ϕ is a stress intensification factor. The exponents, m and n, vary with the rate-limiting mechanism according to Table 2. A slope of a logarithmic plot of the $d\rho/dt$ as a function of grain size at constant pressure should indicate the primary rate-controlling mechanism at each temperature.

Table 2. Associated exponents for hot pressing mechanisms.

Mechanism	Grain Size Exponent, m	Stress Exponent, n
Lattice diffusion	2	1
Grain boundary diffusion	3	1
Plastic deformation	0	≥3
Viscous flow	0	1
Grain boundary sliding or particle rotation	1	1 or 2

Densification rate as a function of grain size at constant temperature and pressure is plotted in Figure 6. The values for the grain size exponent, m, indicate that at lower temperature, grain motion such as sliding and rotation is the limiting

mechanism, although surface diffusion may also contribute significantly. At 0.6 T_m, densification is limited by lattice diffusion and finally by grain boundary diffusion at the upper temperatures.

The corresponding activation energy, Q_{act}, can be determined with an Arrhenius plot of $d\rho/dt$ versus T^{-1}. Figure 7 shows the plots for a 5-nm crystal system at 100 MPa for the various temperatures. The analysis yields linear curves for each temperature. Activation energies are derived from the slopes of the curves. At 0.5 T_m, Q_{ac} is determined to be 63.9 $kJ \cdot mol^{-1}$ which correlates with published values for carbon interstitial and surface diffusion of 58 $kJ \cdot mol^{-1}$. Similarly, the Q_{act} at 0.6 T_m is determined to be 338 $kJ \cdot mol^{-1}$, which corresponds to the reported values for C vacancy diffusion of 338 $kJ \cdot mol^{-1}$. At 0.7 T_m, the calculated Q_{act} of 342 $kJ \cdot mol^{-1}$also corresponds to values for lattice diffusion of Si vacancy (Bockstedte, Mattaausch, and Pankratov 2004).

Lattice diffusion is also observed during the MD simulations. Snapshots from the simulations show abundant lattice defects at temperatures of 0.6 T_m and above. Figure 8 shows the same 10-nm crystal system as shown in Figure 5 at 0.7 T_m. The numerous orange atoms within the crystals indicate point defects that are rarely observed at 0.5 T_m.

4. Conclusions

Recent advancements in sintering, such as FAST techniques, enable the production of nanoscale ceramic materials and possibly nano-composites. However, optimizing these accelerated processes requires a much greater understanding of the governing mechanism than what we currently have. Our approach is to use multi-scale modeling to analyze the conditions that occur in the sintering chamber during processing and to identify the atomic scale mechanism that influence densification under those conditions. The atomistic level simulations to date have revealed several important phenomena, such as that neck formation occurs preferentially between favorably aligned interfaces and does not occur between misaligned interfaces. These results can be used to improve early stage models and current meso-scale models that assume neck formation across all interfaces. Other findings from the MD simulations, such as activation energies, can be used to parameterize these longer length scale models, allowing the meso-scale model to describe grain growth under various sintering conditions.

The intended outcome of this work is to have a continuous multi-scale capability that can be used to enhance our control of the sintering process to produce nano-crystalline ceramic materials with only an acceptable level and type of defects. Such ceramics should rival the strength of steel with greater stiffness and with effective densities comparable to aluminum. Such a material would have revolutionary impact on military logistics.

We point out that the MD simulations of sintering are computationally demanding to the point where a realistic simulations cannot be performed without the capabilities provided be our HPC resources. Any development of larger length scale models aided by MD simulation results would be greatly diminished and nearly impossible without our ability to run these large atomic scale simulations.

Acknowledgements

The authors gratefully acknowledge funding support from the U.S. Army Engineer Research and Development Center research programs “Nanoscale Studies of Polycrystalline Materials with Emphasis on Ceramic Synthesis” and “Multi-Scale Understanding and Engineering of Grain Boundaries in Ceramics,” and the allocation of computer time from the High Performance Computing Challenge Project “Molecular Dynamic Simulations to Underpin the Design and Development of High-Performance Carbon Nanotube based Filaments, Membranes, and Coatings.” We thank the Chief of Engineers for permission to publish this article.

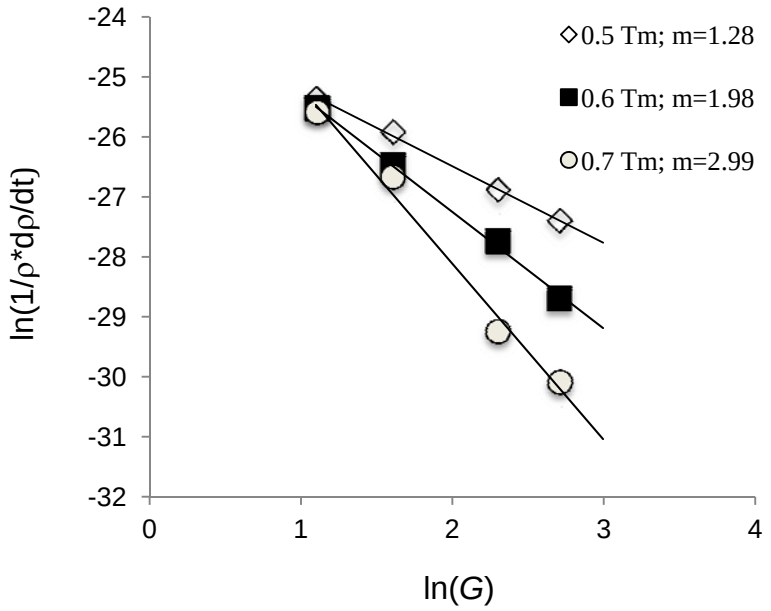

Figure 6. Densification rates as a function of grain size at constant temperature and pressure.

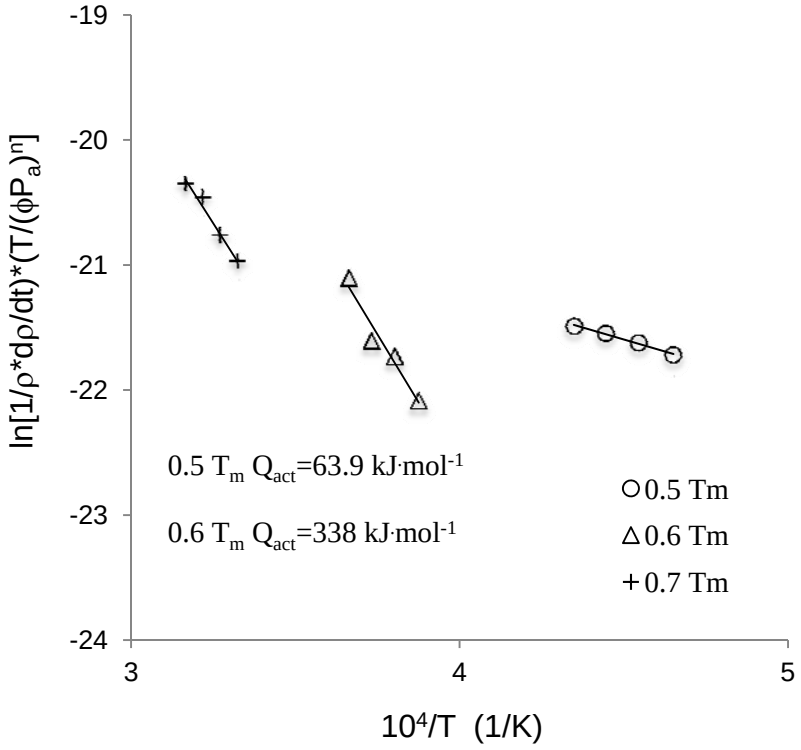

Figure 7. Arrhenius plots of densification rates as a function of T^{-1} at constant temperature and pressure.

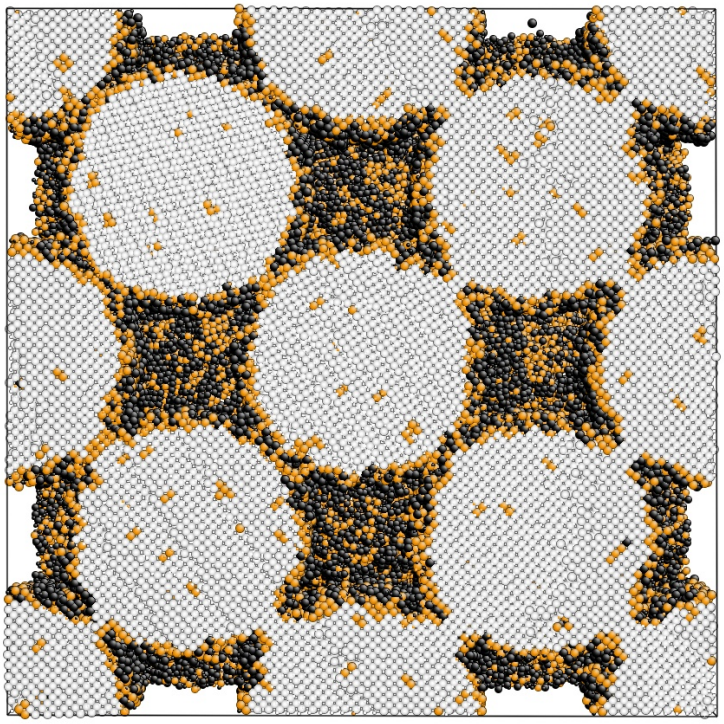

Figure 8. Point defects in 10-nm crystals at 0.7 T_m. Color indicates defects; black atoms are undercoordinated, orange atoms are dislocations or point defects.

References

Allen, J. B., C. F. Cornwell, B. D. Devine, J. F. Peters, and C. R. Welch. "Finite Element Simulations of the Field Assisted Sintering Technique." *Computational Materials Science*, forthcoming.

Bockstedte, M., A. Mattaausch, and O. Pankratov, "*Ab Initio* Study of Annealing of Vacancies and Interstitials in Cubic SiC: Vacancy-Interstitial Recombination and Aggregation of Carbon Interstitials." *Phys. Rev. B.* 69(23), 2004.

Coble, R. L., "Diffusion Models for Hot Pressing with Surface Energy and Pressure Effects as Driving Forces." *J. Appl. Phys.* 41(12), 1970.

Devine, B. D., T. Shan, A. J. McGaughey, S. R. Phillpot, and S. B. Sinnott, "Atomistic Simulations of Copper Oxidation and Cu/Cu_2O Interfaces using COMB Potentials." *Phys. Rev. B.* 84(12), 2011.

Erhart, P., and K. Albe. "Analytical Potential for Atomistic Simulations of Silicon, Carbon, and Silicon Carbide." *Phys. Rev. B.* 71(14), 2005.

Howatson, A. W., P. D. Lund, and J. D. Todd, *Engineering Tables and Data*, New York, Chapman and Hall, 1991.Sharpe, W. N., G. M.

Langer, J., M. J. Hoffmann, and O. Guillon, "Direct Comparison Between Hot Pressing and Electric Field-Assisted Sintering of Submicron Alumina." *Acta Materialia*, 57(18), 2009.

Martyna, G., M. L. Klein, and M. Tuckerman, "Nose-Hoover Chains: The Canonical Ensemble via Continuous Dynamics." *J. Chem. Phys.* 97(4), 1992.

Mo, Y., and I. Szlufarska, "Simultaneous Enhancement of Toughness, Ductility, and Strength of Nanocrystalline Ceramics at High Strain-Rates." *Appl. Phys. Letts.* 90(18), 2007.

Munoz, S. and U. Anselmi-Tamburini, "Temperature and Stress Fields Evolution During Spark Plasma Sintering Processes." *J. Mat. Sci.* 45, 2010

Orru, R., R. Licheri, A. Locci, A. Cincotti, and G. Cao, "Consolidation/Synthesis of Materials by Electric Current Activated/Assisted Sintering." *Mater. Sci. Eng. R* 63, 2009.

Parrinello, M., and A. Rahman, "Polymorphic Transitions in Single Crystals: A New Molecular Dynamics Method." *J. Appl. Phys.* 52(12), 1981.

Petrovic, J.J., D.L Milewski, and F. Rohr, "Tensile Properties of SiC Whiskers." *J. Mat. Sci.* 20,1985

Rahaman, M. N., *Sintering of Ceramics*, Boca Raton, FL, Taylor and Francis, 2008.

Szlufarska, I., A. Nakano, and P. Vashishta, “A Crossover in the Mechanical Response of Nanocrystalline Ceramics.” *Science*, 39, 2005.
Tersoff, J. “Empirical Interatomic Potential for Silicon with Improved Elastic Properties.” *Phys. Rev. B.* 38(14), 1988.